López-Santiago, J. (2018) On the use of wavelets to reveal oscillatory patterns in stellar flare emission. *Philosophical Transactions of the Royal Society A: Mathematical, Physical and Engineering Sciences,* 376(2126), 20170253, pp.: 1-13.

DOI: https://doi.org/10.1098/rsta.2017.0253

PHILOSOPHICAL TRANSACTIONS A

rsta.royalsocietypublishing.org

Research

On the use of wavelets to reveal oscillatory patterns in flaring coronal loops

J. López-Santiago

Department of Signal Theory and Communications, Universidad Carlos III de Madrid, Leganés 28911, Spain

Subject Areas:

Keywords:
Wavelets, Morlet, Stellar Flares, Oscillations, Sun, X-rays

Author for correspondence:
J. Lopez-Santiago
e-mail: jalopezs@ing.uc3m.es

Research on wave propagation along coronal loops was restricted to theoretical approaches for many years, as they were not observed in existing solar data. With the arrival of the new generation solar missions, some of these oscillations could be observed and their characteristics investigated. Propagating waves have been revealed mainly during solar flares so they have been related to plasma evolution inside the loop. Loop waves have been attributed to the MHD evolution of a perturbed magnetic tube. Plasma sloshing has been proposed as a new physical process able to trigger oscillations in coronal loops. In this scenario, the oscillation would be produced by the propagation of a pressure wave caused by a brief, intense energy release at the beginning of the flaring event. Distinguishing between both processes is not easy and the analysis of many events is needed. Nor revealing oscillatory patterns in flare light curves is easy because the oscillation is rapidly attenuated. The use of wavelets is adequate to reveal oscillatory patterns that are localised in time. This work shows some important aspects of the wavelet analysis of stellar flares light curves.

1. Introduction

In the decade of 1980s, solar physicists focussed their attention on a phenomenon causing wave propagation on the solar surface. This phenomenon is currently known as Solar Seismology and comprises propagation of waves in both, photosphere and corona. In the latter, waves propagate along magnetic tubes, the so-called coronal loops and their study provides a way to determine physical parameters of the plasma inside the loop.

THE ROYAL SOCIETY PUBLISHING

Coronal seismology is indeed a powerful tool to investigate basic properties of the solar corona as it provides unique information on coronal physical conditions [1]. From the Magneto-Hydrodynamics (MHD) approach, a coronal loop that is perturbed from its equilibrium state can oscillate in a number of modes (see [2] for a formal treatment of equations). These modes are divided into two categories: trapped modes, which are modes not transmitted outside the tube, and leaky modes, when part of their energy is released into the surrounding medium. The latter experiences damping by radiating waves [3]. The former does not display such acoustic damping [4]. The most common leaky modes studied in literature are sausage and kink modes [5]. Kink modes do not produce changes in the plasma emission measure and so, they do not cause variations in the emitted flux. They are associated to transversal vibrations of the loop to the perpendicular plane containing the loop footprints [6]. Sausage modes are fundamental axisymmetric modes likely produced by internal excitation. According to [7], energy is released instantaneously inside the loop causing an increase in the temperature of the plasma. As a result, plasma kinetic pressure increases, expanding the loop and causing a pulsation when it returns to equilibrium. This pulsation is transmitted onto the energetic electrons, which move downwards along the loop. When those electrons reach the loop footprints, they cause modulated X-ray emission from chromospheric plasma. This explanation is not completely satisfactory because a continuous input of high energy electrons is needed and this is not expected in single loop flaring events. An alternative interpretation is provided by [8]. An increase in the magnetic pressure in the loop alters the pressure equilibrium, modifies its volume and, consequently, the emission measure of the plasma. If the magnetic flux is conserved and the plasma is considered optically thin, the increment in volume is proportional to the decrement in brightness. When the loop returns to equilibrium, it pulses and an oscillatory pattern is observed. Both scenarios predict amplitudes in flux of less than 10% for a typical flaring loop, with temperatures of up to 50 MK, densities $\sim 10^{10}$ cm^2 and magnetic fields of a few hundred Gauss. [9] proposes a different physical process to trigger oscillations inside a coronal loop. Through Hydrodynamic (HD) simulations, the author shows that brief and intense heat pulses are able to develop large amplitude (20% in density) oscillations in flaring loops. The only restriction for the oscillation to occur is that the duration of the heat pulse is shorter than the sound crossing time of the flaring loop. In such scenario, the plasma does not have time to reach pressure equilibrium during heating and traveling pressure fronts develop. The pressure front is reflected at the loop footprint and then, it travels backwards until it reaches the other footprint, where it is again reflected. Due to damping by energy looses, only a few oscillations are observed.

Distinguishing between the different proposed scenarios is required to better understand the physical process triggering oscillations during flares. Oscillatory phenomena have been observed in solar flaring loops at different wavelengths [10–13]. By analogy with the Sun, oscillatory patterns observed during stellar flares are interpreted as the natural MHD evolution of plasma inside the flaring loop [8,14–20]. Attempts in understanding the physical process triggering such oscillations reveal a variety of likely phenomena, from slow magneto acoustic waves [17,21–24] to fast sausage or kink modes [6,11,25–27] or more exotic processes [28]. More observations are needed to unveil the actual mechanism triggering oscillations in those stars.

Wavelet analysis has proven to be suitable to detect oscillations in light curves from solar flares [29]. These oscillations suffer for damping and frequency modulation as the plasma temperature decreases and they are localised in time. Classical Fourier transforms cannot deal effectively with non-stationary signals. Short-time Fourier transforms are a modification of the latter, where a *mask function* (or window) is applied to the signal. The object of this masking is to restrict the analysis of the signal to particular time periods. Thus, the short-time Fourier transform can be used to determine frequencies and/or phases of oscillatory phenomena in local segments of the signal. The disadvantage of the short-time Fourier transform is that it has a fixed resolution for all frequencies. Wide time-windows result in high frequency resolution, as for a classical Fourier transform, while narrow time-windows provide high temporal resolution but low frequency

resolution. If the signal contains both, low and high frequency oscillatory patterns, the short-time Fourier transform must be applied more than once using different windows to reveal each frequency component. Wavelet transforms are introduced to solve this issue. They show high temporal resolution at high frequencies and low temporal resolution at low frequencies. The combined resolution of both is then limited. The wavelet (mother wavelet or mother function) is a time-limited function, contrarily to the sinusoids used in Fourier analysis. A commonly used mother function is the Morlet wavelet. A brief description of this wavelet and its usefulness in detecting non-stationary oscillatory patterns is given in Section 2.

2. Brief description of the Morlet wavelet and its transform

(a) The Morlet wavelet

The Morlet wavelet is a kind of Gabor wavelet, this is, a plane wave localised by a Gaussian window. The expression for the 1-D Gabor wavelet is [30]

$$\Psi_G(t) = e^{-jk_0(t-t_0)} e^{-(t-t_0)^2 a^2} \tag{2.1}$$

where k_0 modulates the frequency and a controls the exponential decay. The 1-D Gabor wavelet does not have orthonormal basis. Its inverse transform cannot be easily reconstructed by a linear superposition. [31] modified the Gabor wavelet to make it satisfy the admissibility condition. This admissibility condition ensures that the inverse transform and Parseval's formula are applicable. The result is the so-called Morlet wavelet [32],

$$\begin{aligned} \Psi_M(t) &= c_\sigma \pi^{-\frac{1}{4}} e^{-\frac{t^2}{2}} \left(e^{j\sigma t} - e^{-\frac{\sigma^2}{2}} \right) \\ c_\sigma &= \left(1 + e^{-\sigma^2} - 2e^{-\frac{3\sigma^2}{4}} \right) \end{aligned} \tag{2.2}$$

whose Fourier transform is

$$\hat{\Psi}_M(\omega) = c_\sigma \pi^{-\frac{1}{4}} \sqrt{2\pi} \left(e^{-\frac{(\sigma-\omega)^2}{2}} - e^{-\frac{\sigma^2}{2}} e^{-\frac{\omega^2}{2}} \right) \tag{2.3}$$

Here, σ is the central frequency of the wavelet. If $\sigma \geq 6$, the second term inside the brackets in $\Psi_M(t)$ (Equation 2.2) is negligible and also the exponentials in c_σ. Then, the Morlet wavelet is simplified to

$$\Psi_M(t) = \pi^{-\frac{1}{4}} e^{-\frac{t^2}{2}} e^{j\sigma t} \tag{2.4}$$

with Fourier transform,

$$\hat{\Psi}_M(\omega) = \pi^{-\frac{1}{4}} \sqrt{2\pi} e^{-\frac{w^2}{2}} e^{-\frac{(\sigma-\omega)^2}{2}} \tag{2.5}$$

This is the usual definition of the Morlet wavelet in the literature [33].

(b) The wavelet transform

The wavelet transform of a continuous-time signal $x(t)$ is determined by

$$W_M(\omega) = \frac{1}{\sqrt{a}} \int_{-\infty}^{+\infty} \Psi_M^* \left(\frac{t-b}{a} \right) x(t)\, dt \tag{2.6}$$

where Ψ_M^* is the complex conjugate of the wavelet and a and b are the scaling and the shifting factor, respectively. For the Morlet wavelet,

$$W_M(\omega) = \frac{1}{\sqrt{a}} \int_{-\infty}^{+\infty} \pi^{-\frac{1}{4}} e^{-\frac{1}{2}\left(\frac{t-b}{a}\right)^2} e^{-j\sigma\left(\frac{t-b}{a}\right)} x(t)\, dt \tag{2.7}$$

The wavelet transform can be understood as a convolution of the signal with the mother wavelet. A family of transforms is obtained by varying the scaling a and shifting b. For low values of a, the wavelet is well localised in frequency, but poorly localised in time. For high values of a, the wavelet is poorly localised in frequency. In other words, the wavelet transform has information in both time and frequency, similarly to a short-time Fourier transform but with variable resolution in both time and frequency domains.

3. Synthetic flare light curves

This work is focussed on the analysis of light curves from solar and stellar flares using wavelet transforms. The Morlet wavelet is used because it has been proven to be able to unveil oscillatory patterns in noisy coronal flare light curves (see Section 1). Such oscillations are difficult to unveil in the time domain but they give invaluable information on the physical properties of the hot plasma confined in coronal loops. To show the powerfulness of the wavelet transform analysis, artificial data are generated in this section. In particular, synthetic light curves with different photon statistics and flare amplitudes are generated. Oscillation patterns with distinct amplitudes are added as a last step. Amplitude damping is reproduced by applying an exponential decay with time:

$$A \propto A_o e^{-t/\tau_o} \tag{3.1}$$

being A_o the initial amplitude of the oscillation and τ_o the decay time. The oscillation is assumed to be a sinusoidal function

$$A \propto A_o e^{-t/\tau_o} \sin \omega t \tag{3.2}$$

with $\omega = 2\pi\nu$ and ν the oscillation frequency ($\nu = 1/T$; T is the oscillation period). To create the flare geometry, rapid exponential rise of the stellar flux is assumed at the first stage of the flare:

$$f = f_0(1 + A_f e^{t/\tau_r}) \tag{3.3}$$

where f_0 is the quiescent flux (the flux before the flaring event), A_f is the flare amplitude and τ_r is the rise time. Then it follows a slow decay with τ_d

$$f = f_0(1 + A_f e^{-t/\tau_d}) \tag{3.4}$$

For the purpose of comparing synthetic results with those of actual stellar light curves, the flare length, rise and decay times are chosen to match those observed in some young stars [8,34,35]: $\tau_r = 5$ ks and $\tau_d = 50$ ks for a total flare duration of 130 ks. An example of a synthetic flare light curve is shown in Fig. 1, left panel. For the oscillation, three different frequencies are analysed. Similarly, three values of τ_o are simulated: 2.5, 5 and 10 ks, corresponding to 0.5, 1 and 2 times the period of the simulated oscillations. This combination of values produces *quality* parameters for the oscillation $Q \sim 6 - 25$, typically observed in solar and stellar flares [8]. Figure 1 (right panel) shows an example of a simulated oscillation with a small amplitude. A summary of the the set of parameters used for the simulations is given in Table 1.

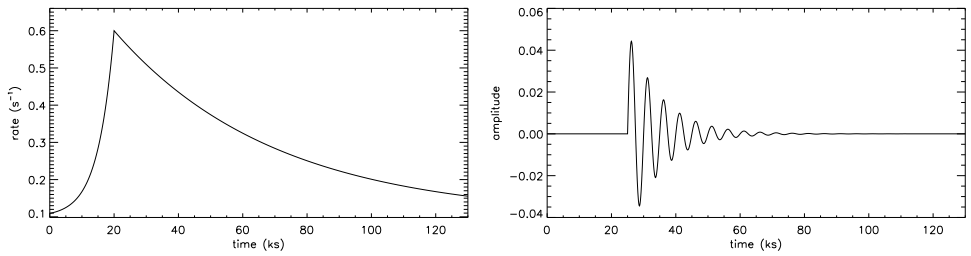

Figure 1. Left: example of a simulated flare light curve with quiescent count-rate 0.1 s^{-1} and flare amplitude 6. Decay time is 50 ks and rise time is 5 ks. **Right:** oscillation with amplitude 50% of the quiescent count-rate assumed in the left panel. Oscillation frequency is 5 ks and damping time is 10 ks. Time binning is 100 s.

Table 1. Grid of parameters used for creating synthetic flare light curves

Parameter	Name	Simulated values	Units
Quiescent rate	cr	0.01/0.1/1.0	s^{-1}
Flare amplitude	A_f	5/10/100	s^{-1}
Oscillation starting time from flare maximum	t_o	-5/+5	ks
Oscillation frequency	P_o	2.5/5.0/10.0	ks
Oscillation amplitude (%)	A_o/A_f	0.15/0.3/0.5	...
Damping time	τ_o	2.5/5.0/10.0	ks

I include noise in the analysis to understand its role in the wavelet power spectrum. The procedure by [36] is followed to generate random Poissonian deviations for each point of the curve. Let $N = N_0 e^{-\lambda t}$ be a photon counting process (Poisson distributed) with a relaxation rate λ. Its power spectrum is then a Lorentzian function

$$S(\omega) = \frac{N_0^2 n}{\lambda^2 + \omega^2} \tag{3.5}$$

where n is the average pulse rate and $\omega = 2\pi\nu$, being $\nu = 1/t$ the sampled frequency. When $\lambda << \nu$, $S(\nu) \propto 1/\nu^2$ (i.e. red noise). Contrarily, $S(\nu) = N_0 n$ when the relaxation time $\lambda >> \nu$ (constant power spectrum ore white noise).

4. Wavelet power spectrum of ideal light curves (noise-free)

The power spectrum of the wavelet transform is defined as $|W_M(\omega)|^2$. Like the wavelet transform, the wavelet power spectrum is a 2D function, being time and frequency the two independent variables. Features in the temporal sequence (jumps, discontinuities, periodicity, ...) are revealed in $|W_M(\omega)|^2$ as significant peaks. In particular, sinusoid-type signals are shown in the power spectrum as strips localised in frequency and expanding in time for the duration of the oscillation. Figure 2 shows a synthetic light curve of a typical flare with a sinusoidal pattern added after the maximum rate, and its wavelet power spectrum. The period of the sinusoid is 5000 s and the starting time is 25000 s. The sinusoid is localised in frequency, at $P = 5000 \pm 1000$ s ($\omega = 1.25 \pm 0.25 \times 10^{-3}$ rad s^{-1}). Contrarily, the global shape of the light curve caused by the rapid increase and gradual exponential decrease emission during the flaring event extends in frequency below $\omega = 2\pi/10^4$ rad s^{-1} ($P > 10000$ s).

The typical scenario observed in solar and stellar flares is, instead, an oscillation with varying amplitude with time due to the lost of energy. Figure 3, shows a set of models of a flare light curve with different oscillation patterns together with their wavelet power spectrum. For the purpose of visually comparing the effect of increasing the amplitude of the oscillation without changing

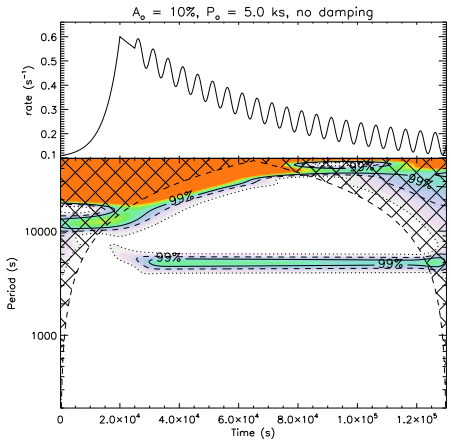

Figure 2. Simulation of a flare like curve with a low amplitude oscillation ($A_o/A_f = 10\%$) with period $P_o = 5$ ks and no damping. Parameters of the flare light curve are as in Figs. 1. Time binning is 100 s. Dotted line is for confidence level 66%, dashed line is for 95% confidence level and continuous line is for 99% confidence level.

the frequency, I plot two pairs of rows: the first and second rows correspond to sets of simulations assuming amplitudes of 15% and 30%, respectively, and an oscillation period of 2.5 ks. The third and fourth rows are like the first and second rows, respectively, but for an oscillation period of 5 ks. From left to right, each row shows simulations with increasing oscillation decay time (damping; 2.5, 5 and 10 ks, respectively; see top label in each panel of the figure). Cross-hatched regions in the wavelet power spectrum indicate the cone of influence, where edge effects become important. I plot contours for 67, 95 and 99% confidence levels (dotted, dashed and continuous lines, respectively). The confidence levels are determined following Section 4.c, Eq. 18 of [33], assuming a constant background spectrum in the wavelet, i.e. $P_k = 1$ in their equation. This chose is justified because no noise is added to the time series at this stage.

As expected, the amplitude of the oscillation is an important factor for detecting it at a high confidence level. Simulations with oscillation amplitude $A_o/A_f = 0.3$ (30% of the count-rate just before the oscillation) are detected at a confidence level $> 95\%$, independently of the frequency of the oscillation and the damping time, while oscillations with amplitude $A_o/A_f = 0.15$ (15% of the flux before the oscillation) are not detected at such confidence level. The effect of the damping on the detection of the oscillation is to reduce the time period of high significance in the wavelet power spectrum. This behaviour is evident in, e.g. the simulations shown in the second row of Fig. 3, where the oscillation amplitude and frequency are fixed while the damping time varies from 2.5 to 10 ks (from left to right). This result is related to the number of oscillation periods/peaks observed well above the unperturbed flare light curve. If the oscillation is not damped, the peak in the wavelet extends over the entire duration of the observation (see Fig. 2).

5. Effect of Poisson noise on the wavelet transform

In any physical process of photon emission, Poisson noise is usually dominant when the number of photons detected is small. In such a case, the occurrence of independent random events is described by a Poisson distribution. X-ray Astronomy is a clear example, since photon-rates are low for many sources. Poisson noise is also amplified in photodetectors, which use to have quantum efficiency below unity. Therefore, understanding the effect of noise in the wavelet transform is necessary.

Noise is added to the simulations in the previous section by generating random Poissonian deviations following the procedure by [36]. The resultant light curve is analysed using the wavelet

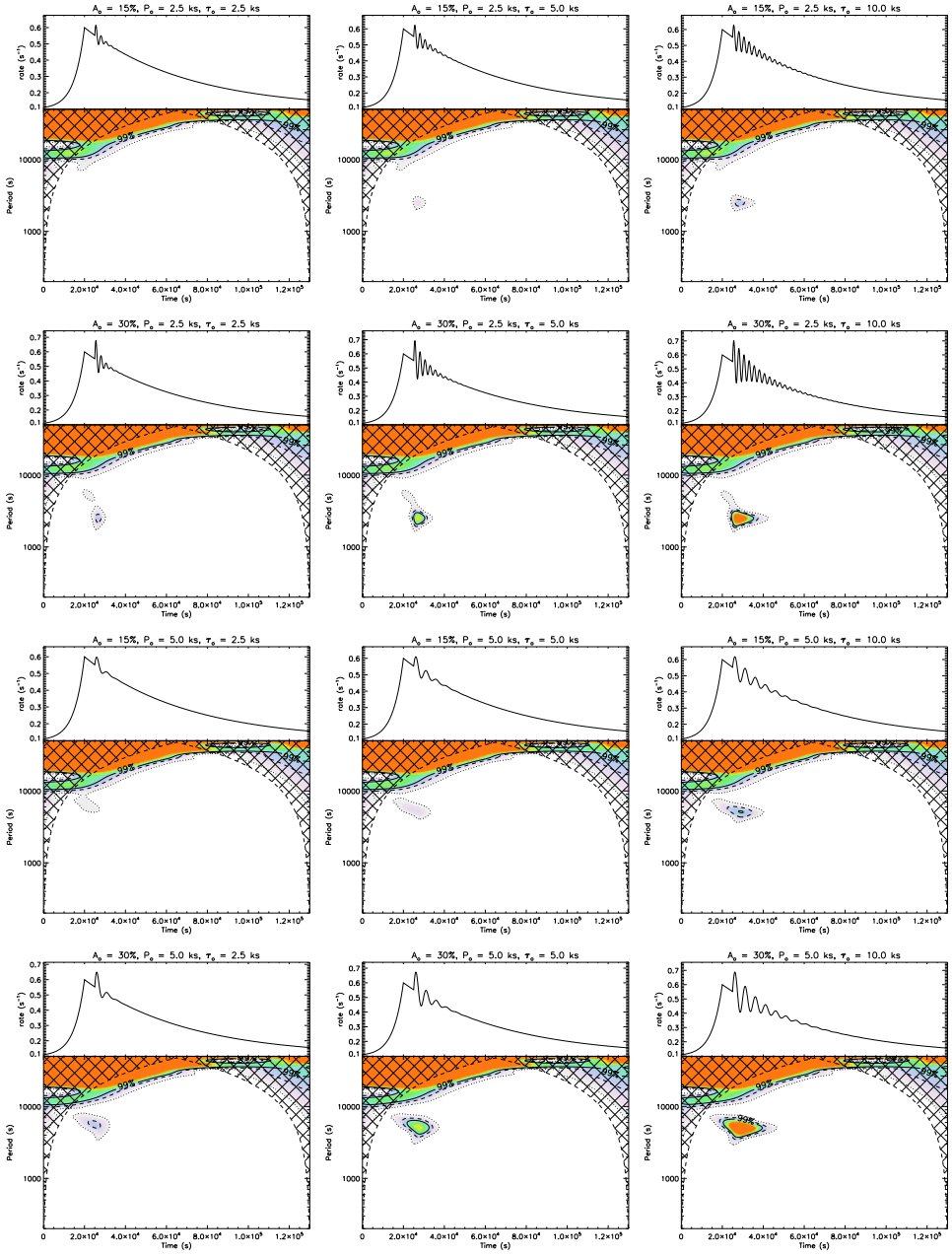

Figure 3. Set of simulations without noise. Each row shows simulations of an oscillation with the same frequency but different damping-decay time (from left to right, $\tau_o = 2.5, 5, 10$ ks). First and second rows show simulations with oscillation frequency 2.5 ks but different amplitude (15% and 30%, respectively). Third and fourth rows are as first and second row, respectively, but with an oscillation frequency of 5 ks. Time binning is 100 s in every case. The contours are 66%, 95% and 99% confidence level for dotted, dashed and continuous line, respectively

transform, as in Section 4. An example of the resultant wavelet power spectra is shown in Fig. 4. The effect of noise is to change the global spectrum, i.e. to enhance the background spectrum. As a result, the significance of peaks in the wavelet spectrum is modified. In addition, other spurious peaks close to that of the actual oscillation may appear in the power spectrum. The set of

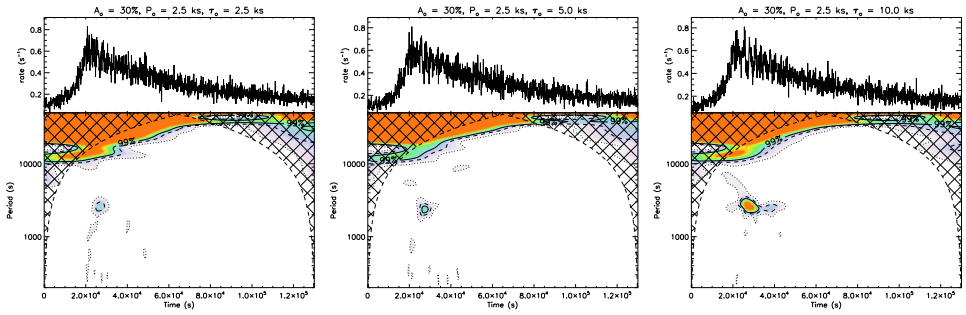

Figure 4. Set of simulations including noise. Light curve aspect and oscillation patterns are as in the second row of Fig. 3. Time binning is 100 s.

simulations shown in Fig. 4 is similar to the second row of Fig. 3, i.e. flare with amplitude $A_f = 5$ and different oscillation patterns, but including also Poison noise. The peaks are still present. However, the wavelet spectrum is noisier, in general. In some cases, another features with a lower confidence level appear close to the actual oscillation period. These other features are spurious and are a product of noise. This result is independent of the starting time of the oscillation.

To analyse whether pure noise in a flare light curve may produce high confidence levels in the wavelet power spectrum, Montecarlo methods are used to create a thousand simulations including Poisson noise but without any oscillation pattern. Two scenarios are checked: *i)* high count-rate and *ii)* low count-rate, simulating high and low signal-to-noise ratio observations, respectively. In both cases, the light curve is simulated using the same parameters than in the previous section (Fig. 1). For the high count-rate scenario, $cr = 0.1$ s^{-1} is used. For the low count-rate scenario, $cr = 0.01$ s^{-1} is used. In the high count-rate scenario, only 1% of the simulations show a confidence level above 99% in the period range analysed, while 23% of the simulations show at least one peak with a confidence level $\sim 95\%$. In the case of low count-rate, the percentage of simulations showing peaks at the 99% confidence level reaches the 88%, while the 100% of them show peaks at the 95% confidence level. Thus, for low count-rate (low signal-to-noise), it is easy to obtain spurious peaks in the wavelet power spectrum at large confidence levels. For light curves with high count-rates (high signal-to-noise ratio), the probability of detecting spurious peaks in the wavelet power spectrum is low. Similar results are obtained for simulations of flare light curves with low amplitude at the flare maximum. For instance, for a count-rate of 0.1 s^{-1} and a flare amplitude of 3 (instead of 5) only 4% of the simulations show peaks at the 99% confidence level.

From the analysis of Sections 4 and 5, it may be concluded that oscillatory patterns with amplitudes $> 10\%$ in flare light curves are clearly detected through a wavelet analysis but spurious peaks caused by Poisson noise may be misled as oscillation patterns in light curves with low photon statistics. This result is complementary to that obtained by [37]. There, the authors demonstrate that a pure random red noise time series may produce peaks in the power spectrum whose power exceeds the 3σ confidence level. Here, I show that Poisson noise produces this effect in flare light curves with low photon statistics.

6. Application to AT Mic

The wavelet power spectrum of a flare observed in X-rays in the M dwarf AT Mic was investigated by [17]. In their work, the authors follow the method described in [33]. From their analysis, [17] deduce that the flaring loop in AT Mic likely underwent an oscillation with a period of 750 s. The authors present this result as the first oscillation observed in X-rays in a star different from the Sun.

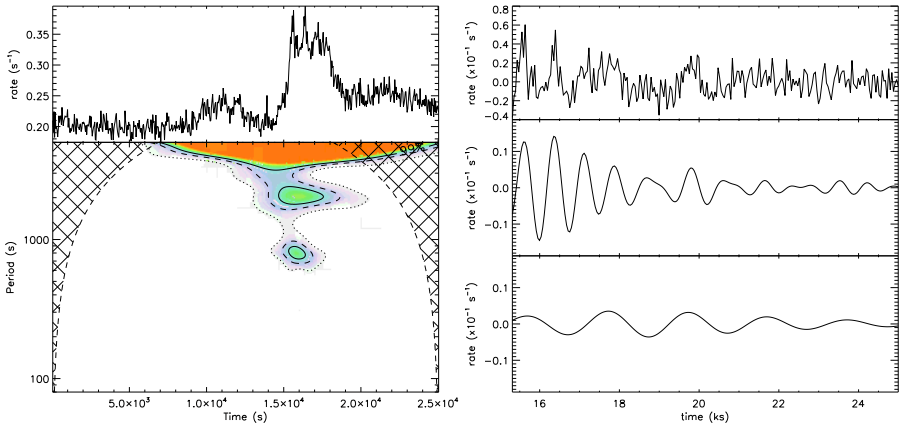

Figure 5. Left: wavelet power spectrum (bottom sub-panel) of the X-ray light curve of AT Mic (top sub-panel). The temporal binning is 40 s. The two peaks at 95% confidence levels are $P = 800$ and 2000 s, respectively. **Right:** de-trended signal in the time period $15\ ks < t < 25\ ks$ (top sub-panel), filtered signal for $600\ s < P < 900\ s$ (mid sub-panel) and filtered signal for $1800\ s < P < 2200\ s$ (bottom sub-panel).

Figure 5 shows the wavelet power spectrum of the light curve of AT Mic. The temporal bin is 30 s instead of the 10 s used by [17]. As it is shown in [33], smoothing the wavelet power spectrum can be used to enhance confidence levels in regions of significant power. With this approach, two peaks are detected in the wavelet power spectrum (top panel in Fig. 5) with confidence levels above 99%: the $P \approx 800$ s pattern already detected by [17] and a second one at $P \approx 2000$ s. This second pattern corresponds to a global, low-amplitude oscillation that is more evident in the de-trended light curve. Right panel in Fig. 5 shows the de-trended light curve of AT Mic during the flaring event. A simple moving average with a width of 1800 s is subtracted to remove the global flare pattern. The other two panels in that figure are the result of filtering the light-curve with an ideal band-pass filter centred at $P = 750$ s and $P = 2000$ s, respectively. The filter has frequency amplitude $\Delta\nu = 0.4$ mHz ($\Delta P = 150$ s) for the feature at $P = 750$ s and $\Delta\nu = 0.1$ mHz ($\Delta P = 200$ s) for the feature at $P = 2000$ s.

In Section 4, it was shown that the global shape of the flare light curve is not localised in time or frequency. In particular, the power spectrum of the rapid increase and later slow exponential decrease of intensity caused by the flare extends towards low frequency from a given value. In the flare analysed here, the global baseline is clearly revealed at $\omega > 2\pi/3000$ rad s^{-1} ($P > 3000$ s). Thus, it seems adequate to filter the original dataset using a high-pass filter with this cut frequency to keep only the oscillatory pattern. The result of applying this filter is shown in Figure 6. The power of the two peaks are similar, indicating the high significance of the long period oscillation too. Instead, the power of the (high frequency) noise is low.

The example shown in this section demonstrates that the wavelet analysis is a powerful tool to reveal oscillations in stellar light curves, particularly after flaring events. A previous treatment of the signal by, for example, filtering the data using a high-pass filter enhances the significance of the detected features. It is also shown that the original light curve can be reconstructed from the power spectrum and, in particular, any oscillation can be identified from the wavelet spectrum by filtering the frequencies where the oscillation is not revealed.

7. Remarks and conclusions

This work shows the powerfulness of wavelet analysis to reveal non-stationary, oscillatory patterns in solar and stellar flare light curves. These oscillations develop during the first stages of

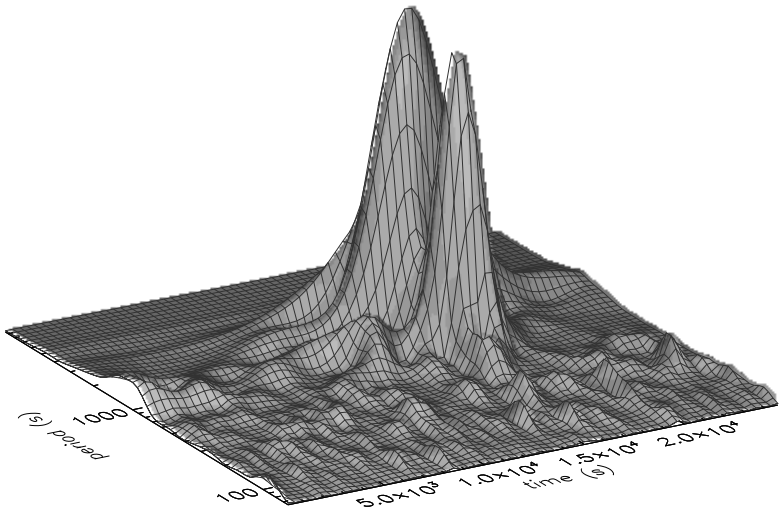

Figure 6. Wavelet power spectrum of the filtered X-ray light curve of AT Mic.

the flaring event and show low amplitudes compared to the global flux enhancement caused by the flare. They are frequency modulated and last only for a few periods (typically 4 to 5 periods). Therefore, flare oscillations are localised in time and frequency. Natural and instrumental noise can mask them in the time domain due to their low amplitude. The Morlet wavelet is particularly well suited to detect damped sinusoids in the frequency domain.

Simulations used for this work show different scenarios with parameters for the oscillation comprising a wide range of values. In every simulation, the wavelet power spectrum reveals the presence of the oscillation. The extension in time of the features revealed in the power spectrum depends on the number of periods observed. For example, if the amplitude of the oscillation decreases with time, it will be localised in time in the wavelet power spectrum (see Fig. 3). Contrarily, if the oscillation is not damped, its power spectrum will look like that shown in Fig. 2. Simulations also help in understanding the role of noise in the wavelet power spectrum. The main effect of noise in the wavelet power spectrum is reducing the significance of the detected features (Section 5). However, the oscillations are still revealed in the frequency domain, at a lower significance level. Choosing the correct noise model is important to determine robust confidence levels. Using simple white noise is wrong for most problems. Many natural processes are controlled by frequency dependent noise (Section 3). This is particularly evident for the scenario analysed in this work. In Section 5 it is shown that Poison noise can produce significant peaks in the wavelet power spectrum. Assuming a white noise background spectrum would detect such peaks as actual patterns in the dataset. Choosing a frequency dependent background spectrum avoids misleading these peaks as oscillations in the observed light curve.

Data treatment previous to the wavelet analysis may be performed to enhance significant features in the wavelet power spectrum. Time binning or smoothing is one frequently used [33]. Baseline filtering is commonly applied when a global, low frequency signal is present. Usually, a simple polynomial fitting is enough to de-trend the signal [8]. A moving average is sometimes used for this purpose (for a brief summary of baseline filtering techniques, the reader is referred

to [38]). Nevertheless, the baseline of the original dataset can be also removed using an ideal band-pass filter in the frequency domain [19]. This approach is applied to a real case in Section 6, as an example. The wavelet analysis method is applied to an X-ray light curve of the M dwarf AT Mic in this paper. This solar-like star underwent a large flare during the *XMM-Newton* observations in October, 2000. The wavelet power spectrum of the X-ray light curve shows three significant features. Two of them are localised in time (they extend only for a few kilo-seconds) and in frequency. The third one is not localised in time and it extends from $\omega \approx 2 \times 10^{-3}$ rad s^{-1} to lower frequencies. This unlocalised feature is related to the global X-ray variability and can be filtered using an ideal high-pass filter. After filtering, the significance of the other two features is enhanced (Fig. 6). These two features likely correspond to the fundamental mode and first harmonic of an oscillation triggered by the flaring event. The two sinusoids can be reconstructed using a band-pass filter for each mode and then, by using an inverse wavelet transform (Fig. 5, right panel).

The results presented in this paper show that a careful wavelet analysis, which may include previous treatment of the data such as band-pass filtering, is a powerful tool to reveal oscillations during stellar flares. Their detection and analysis is helping in determining the properties of the hot plasma inside the coronal magnetic loops.

Data Accessibility. AT Mic X-ray data used in this work are available within the data archive of the *XMM-Newton* space mission through the XSA application: http://nxsa.esac.esa.int/nxsa-web/#search.

Competing Interests. 'The author declares that he has no competing interests'.

Funding. Office of Naval Research Global, award no. N62909-15-1-2011

Acknowledgements. The author acknowledges F. Reale, G. Micela and S. Sciortino for fruitful discussion on the topic. The author also acknowledges I. Crespo-Chacón for previous contribution in simulating light curves.

References

1. Nakariakov, V. M., & Verwichte, E. 2005 Coronal Waves and Oscillations. *LRSP* **2**, 3. (https://doi.org/10.12942/lrsp-2005-3)
2. Stepanov, A. V., Zaitsev, V. V., & Nakariakov, V. M. 2012 Resonators for MHD Oscillations in Stellar Coronae, pp. 39-66. In *Coronal Seismology: Waves and Oscillations in Stellar Coronae*. Wiley-VCH Verlag GmbH & Co. KGaA, Weinheim, Germany, 2012 (https://doi.org/10.1002/9783527645985)
3. Spruit, H. C. 1982 Propagation speeds and acoustic damping of waves in magnetic flux tubes. *Sol. Phys.* **75**, 3. (https://doi.org/10.1007/BF00153456)
4. Edwin, P. M., & Roberts, B. 1983 Wave propagation in a magnetic cylinder. *Sol. Phys.* **88**, 179. (https://doi.org/10.1007/BF00196186)
5. Terradas, J., Andries, J., & Goossens, M. 2007, On the Excitation of Leaky Modes in Cylindrical Loops. *Sol. Phys.* **246**, 231. (https://doi.org/10.1007/s11207-007-9067-6)
6. Nakariakov, V. M., Ofman. L., DeLuca, E. E., Roberts, B., & Davila, J. M. 1999 TRACE Observation of Damped Coronal Loop Oscillations: Implications for Coronal Heating. *Science* **285**, 5429, 862. (https://doi.org/10.1126/science.285.5429.862)
7. Zaitsev, V. V., & Stepanov, A. V. 1982 On the Origin of the Hard X-Ray Pulsations during Solar Flares. *Soviet Astronomy Letters* **8**, 132
8. López-Santiago, J., Crespo-Chacón, I., Flaccomio, E., Sciortino, S., Micela, G., & Reale, F. 2016 Star-disk interaction in classical T Tauri stars revealed using wavelet analysis. *A&A*, **590**, A7. (https://doi.org/10.1051/0004-6361/201527499)
9. Reale, F. 2016 Plasma Sloshing in Pulse-heated Solar and Stellar Coronal Loops. *ApJ*, **826**, L20. (https://doi.org/10.3847/2041-8205/826/2/L20)
10. Klassen, A., Aurass, H., & Mann, G. 2001 Sawtooth oscillations in solar flare radio emission. *A&A*, **370**, L41. (https://doi.org/10.1051/0004-6361:20010332)
11. Inglis, A. R., & Nakariakov, V. M. 2009 A multi-periodic oscillatory event in a solar flare. *A&A*, **493**, 259. (https://doi.org/10.1051/0004-6361:200810473)
12. Nakariakov, V. M., Foullon, C., Myagkova, I. N., & Inglis, A. R. 2010 Quasi-Periodic Pulsations in the Gamma-Ray Emission of a Solar Flare. *ApJ*, **708**, L47 (https://doi.org/10.1088/2041-8205/708/1/L47)

13. Cho, I.-H., Cho, K.-S., Nakariakov, V. M., Kim, S., & Kumar, P. 2016 Comparison of Damped Oscillations in Solar and Stellar X-Ray flares. *ApJ*, **830**, 110. (https://doi.org/10.3847/0004-637X/830/2/110)
14. Bastian, T. S. 1990 Radio emission from flare stars. *Sol. Phys.*, **130**, 265. (https://doi.org/10.1007/BF00156794)
15. Zhilyaev, B. E., Romanyuk, Ya. O., Verlyuk, I. A., Svyatogorov, O. A., Khalack, V. R., Sergeev, A. V., Konstantinova-Antova, R. K., Antov, A. P., Bachev, R. S., Alekseev, I. Yu., et al. 2000 Detection of high-frequency optical oscillations on the flare star EV Lacertae. *A&A*, **364**, 641.
16. Mathioudakis, M., Seiradakis, J. H., Williams, D. R., Avgoloupis, S., Bloomfield, D. S., & McAteer, R. T. J. 2003 White-light oscillations during a flare on II Peg. *A&A*, **403**, 1101. (https://doi.org/10.1051/0004-6361:20030394)
17. Mitra-Kraev, U., Harra, L. K., Williams, D. R., & Kraev, E. 2005 The first observed stellar X-ray flare oscillation: Constraints on the flare loop length and the magnetic field. *A&A*, **436**, 1041. (https://doi.org/10.1051/0004-6361:20052834)
18. Welsh, B. Y., Wheatley, J., Browne, S. E., Siegmund, O. H. W., Doyle, J. G., O'Shea, E., Antonova, A., Forster, K., Seibert, M., Morrissey, P., et al. 2006 *A&A*, **458**, 921. (https://doi.org/10.1051/0004-6361:20065304)
19. Mathioudakis, M., Bloomfield, D. S., Jess, D. B., Dhillon, V. S., & Marsh, T. R. 2006 The periodic variations of a white-light flare observed with ULTRACAM. *A&A*, **456**, 323. (https://doi.org/10.1051/0004-6361:20054752)
20. Pillitteri, I., Wolk, S. J., López-Santiago, J., Günther, H. M., Sciortino, S., Cohen, O., Kashyap, V., & Drake, J. J. 2014 The Corona of HD 189733 and its X-Ray Activity. *ApJ*, **785**, 145. (https://doi.org/10.1088/0004-637X/785/2/145)
21. Selwa, M., Murawski, K., & Solanki, S. K. 2005 Excitation and damping of slow magnetosonic standing waves in a solar coronal loop. *A&A*, **436**, 701. (https://doi.org/10.1051/0004-6361:20042319)
22. Jess, D. B., Pascoe, D. J., Christian, D. J., Mathioudakis, M., Keys, P. H., & Keenan, F. P. 2012 The Origin of Type I Spicule Oscillations. *ApJ*, **744**, L5 (https://doi.org/10.1088/2041-8205/744/1/L5)
23. Anfinogentov, S., Nakariakov, V. M., Mathioudakis, M., Van Doorsselaere, T., Kowalski, A. F. 2013 The Decaying Long-period Oscillation of a Stellar Megaflare. *ApJ*, **773**, 156. (https://doi.org/10.1088/0004-637X/773/2/156)
24. Srivastava, A. K., Lalitha, S., & Pandey, J. C. 2013 Evidence of Multiple Slow Acoustic Oscillations in the Stellar Flaring Loops of Proxima Centauri. *ApJ*, **778**, L28 (https://doi.org/10.1088/2041-8205/778/2/L28)
25. Aschwanden, M. J. 1987 Theory of radio pulsations in coronal loops. *Sol. Phys.* **111**, 113. (https://doi.org/10.1007/BF00145445)
26. Pandey, J. C., & Srivastava, A. K. 2009 Observations of X-Ray Oscillations in ξ Boo: Evidence of a Fast-Kink Mode in the Stellar Loops. *ApJ*, **697**, L153. (https://doi.org/10.1088/0004-637X/697/2/L153)
27. Hindman, B. W., & Jain, Rekha 2012 Axisymmetric Scattering of p Modes by Thin Magnetic Tubes. *ApJ*, **746**, 66. (https://doi.org/10.1088/0004-637X/746/1/66)
28. Gómez de Castro, A. I., López-Santiago, J., Talavera, A., Sytov, A. Yu., & Bisikalo, D. 2013 XMM-Newton Monitoring of the Close Pre-main-sequence Binary AK Sco. Evidence of Tide-driven Filling of the Inner Gap in the Circumbinary Disk. *ApJ*, **766**, 62. (https://doi.org/10.1088/0004-637X/766/1/62)
29. Aschwanden, M. J., Kliem, B., Schwarz, U., Kurths, J., Dennis, B. R., & Schwartz, R. A.1998 Wavelet Analysis of Solar Flare Hard X-Rays. *ApJ*, **505**, 941 (https://doi.org/10.1086/306200)
30. Gabor, D. 1945 Theory of Communication. Part 1: The analysis of information *Journal of the Institution of Electrical Engineers*, **99**, 26. (https://doi.org/10.1049/ji-3-2.1946.0074)
31. Goupillaud, P., Grossman, A., & Morlet, J. 1984 Cycle-Octave and Related Transforms in Seismic Signal Analysis. *Geoexploration*, **23**, 85. (https://doi.org/10.1016/0016-7142(84)90025-5)
32. Addison, P. S. 2017 Complex wavelets: the Morlet wavelet, p. 34. In *The Illustrated Wavelet Transform Handbook: Introductory Theory and Applications in Science, Engineering, Medicine and Finance*. Taylor & Francis Group LCC, CRC Press, 6000 Broken Sound Park Way NW, Suite 300 Boca Raton, Florida, USA, 2017 (ISBN-10: 0750306920)
33. Torrence, C., & Compo, G. P. 1998 A Practical Guide to Wavelet Analysis. *Bull. Amer. Meteor. Soc.*, **79**, 61. (https://doi.org/10.1175/1520-0477(1998)079<0061:APGTWA>2.0.CO;2)

34. Favata, F., Flaccomio, E., Reale, F., Micela, G., Sciortino, S., Shang, H., Stassun, K. G., & Feigelson, E. D. 2005 Bright X-Ray Flares in Orion Young Stars from COUP: Evidence for Star-Disk Magnetic Fields? *ApJS*, **160**, 469. (https://doi.org/10.1086/432542)
35. Getman, K. V., Feigelson, E. D., Micela, G., Jardine, M. M., Gregory, S., G., & Garmire, G. P. 2008 X-Ray Flares in Orion Young Stars. II. Flares, Magnetospheres, and Protoplanetary Disks. *ApJ*, **688**, 437. (https://doi.org/10.1086/592034)
36. Press,W. H., Teukolsky, S. A., Vetterling, W. T., & Flannery, B. P. 2002 Random Numbers, pp. 340-418. In *Numerical recipes in C++: the art of scientific computing*. Cambridge University Press, 32 Av. of the Americas, New York, NY, 10013-2473, USA. (ISBN: 0521750334)
37. Gruber, D., Lachowicz, P., Bissaldi, E., Briggs, M. S., Connaughton, V., Greiner, J., van der Horst, A. J., Kanbach, G., Rau, A., Bhat, P. N., et al. 2011 Quasi-periodic pulsations in solar flares: new clues from the Fermi Gamma-Ray Burst Monitor. *A&A*, **533**, A61. (https://doi.org/10.1051/0004-6361/201117077)
38. Kaur, M., Singh, B., & Seema 2011 Comparisons of Different Approaches for Removal of Baseline Wander from ECG Signal. *IJCA*, **5**, A5. (https://doi.org/10.1145/1980022.1980307)